ESTABLISHMENT AND APPLICATION OF SOIL FERTILIZATION PRESCRIPTION CHART
/
土壤施肥处方图的建立和应用

Fanxia KONG*[1)], Haozheng SUN[1)], Jiankun LI[3)], Baixu LIU[1)], Lili YI[1)], Yubin LAN[1,2)], Xin HAN[1)], Duanyang GENG[1)], Qiang GAO[3)]

[1)]School of Agricultural Engineering and Food Science, Shandong University of Technology, Zibo/ China
[2)]Shandong Provincial Engineering Technology Research Centre for Agricultural Aviation Intelligent Equipment, Zibo/ China
[3)] Weichai Lovol Intelligent Agricultural Technology Co. Ltd, Weifang/ China
Tel:+8618653372858;E-mail: kfx0309@163.com
Corresponding author: Fanxia Kong
DOI: https://doi.org/10.35633/inmateh-72-01

***Keywords**: soil characteristics; soil fertilization prescription chart; spatial interpolation; variable rate fertilization*

ABSTRACT
Precision soil fertilization is an important aspect of smart precision agriculture development, and the fertilization prescription map is a prerequisite for precision fertilization. Taking grapevine soil information as an example, this study explores the impact of different sampling densities on the accuracy of soil nutrient distribution. Experimental trials were conducted using sampling densities of 1m x 1m, 3m x 3m, 6m x 6m, 9m x 9m, and 12m x 12m, with the optimal sampling density determined to be 6m x 6m. Nutrient distribution maps were created using Bigemap and ArcGIS software, and based on nutrient balance calculations using ArcGIS software, fertilization prescription maps were developed. Furthermore, precise fertilization schemes for nitrogen, phosphorus, and potassium fertilizers were formulated based on the prescription maps. This study provides methodological and data support for research on precision soil fertilization.

摘要
土壤精准施肥是智慧精准农业发展的重要方面，施肥处方图是精准施肥的前提。本文以葡萄园土壤信息为例，探索了不同采样密度对土壤养分分布准确度的影响，以 1m x 1m, 3m x 3m, 6m x 6m, 9m x 9m, and 12m x 12m, 为例进行了试验，确定了最佳采样密度为 6m x 6m，使用 Bigemap 和 ArcGIS 软件绘制了养分分布图，根据养分平衡法运用 ArcGIS 软件得出相应的施肥处方图，并基于处方图给出了氮、磷、钾三种肥料的精准施肥方案，为土壤精准施肥研究提供了方法支持和数据支持。

INTRODUCTION
Precision agriculture represents the future trend in agricultural production, with precise soil fertilization being a crucial component of smart farming. China has made significant strides in the development of precise fertilization prescription charts *(An et al., 2017)*, fertilization control algorithms *(Liu et al., 2021; Zhang et al., 2021)*, as well as fertilization systems and mechanisms *(Bai et al., 2021; Jin et al., 2018; Li et al., 2016; Shi et al., 2017; Yuan et al., 2014)*. Moreover, international research efforts have also contributed to advancements in precise fertilization *(Chung et al., 2018; Kabir et al., 2018; Marius et al., 2021; Saleem et al., 2013; Reyes et al., 2015; Yang., 2001)*. The acquisition of fertilization prescription charts is fundamental to precision fertilization.

Currently, research in various aspects of precision fertilization, including the accuracy of prescription charts, efficiency of acquisition, acquisition costs, and the reliability of precision fertilization plans, falls short of meeting the demands of smart precision agriculture development. *Xu et al., (2011),* used Web Services, metadata, spatial interpolation and AJAX technologies, combined with VS2005, ArcGIS 9.3 and SQL Server 2005 and other software, in their paper. NET platform built "WebGIS based wheat precision fertilization decision system", realized the production of wheat prescription map. *Yuan et al., (2013),* studied the soil sampling strategy and the generation method of nutrient distribution map. One soil sample was selected every 10 ridges, and one soil sample was taken from each ridge at an interval of 10 m. The national standard method and rapid measurement method were used to detect the nutrient content. However, the traditional methods of soil sample collection and laboratory testing are not only time-consuming and laborious, but also costly. This can be difficult to achieve for large areas of farmland, limiting the popularity of precision fertilization techniques.

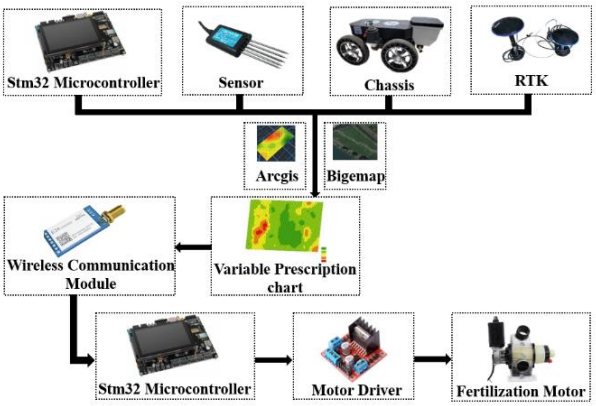

Fig. 1 – System frame diagram

The system frame diagram of this paper is shown in the Fig 1. To address the issue of low efficiency in soil information collection for precision fertilization prescription maps, this study employs an STM32 microcontroller, soil sensors, and Real-Time Kinematic (RTK) technology mounted on a chassis to collect soil information and create fertilization prescription maps. The study investigates the impact of different sampling densities on the accuracy of soil nutrient distribution and determines the optimal sampling density. The prescription map files are transmitted wirelessly to the fertilizer motor control system to achieve variable rate fertilization by controlling the motor speed. This research provides a cost-effective data acquisition method and a more accurate precision fertilization scheme for soil precision fertilization, thereby advancing the development of precision agriculture.

MATERIALS AND METHODS

Soil information collection system

There are various methods for detecting soil information *(Yang et al., 2010; Zhai et al., 2022)*, and in this study, an indirect measurement approach based on soil electrical conductivity was chosen due to its rapid response, cost-effectiveness, and durability. It has been selected a sensor that measures soil nutrient values through electrical conductivity to establish a soil information collection system.

It was opted for the high-precision, rapidly responsive JXBS-3001-TR soil comprehensive sensor in our soil information collection system. This sensor exhibits high accuracy, fast response times, stable output, and is minimally influenced by soil salinity, making it suitable for various soil types. The sensor operates within a voltage range of 12-24V and can withstand temperatures from -40°C to 80°C, thereby complying with our experimental environmental requirements.

The soil information collection system comprises an STM32f429IGT6 development board and the soil comprehensive sensor. It incorporates the SP3485 level-shifting chip and a power module, with sensor readings displayed via a 4.3-inch RGB LCD touch screen module. The hardware configuration features a 485 bus interface, with the sensor functioning as a slave device and its device address set to 0x01. The hardware connection of the system is illustrated in Fig 2.

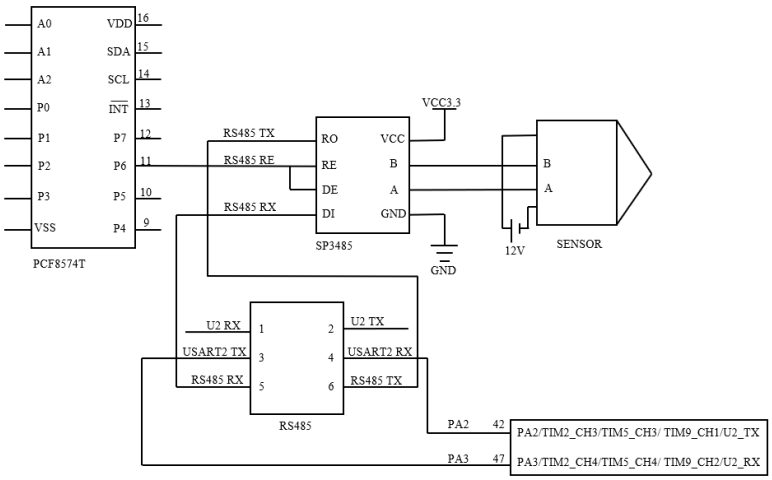

Fig. 2 – Hardware connection chart

In the process of communication between the sensor and the development board, it is essential to predefine various parameters of the communication protocol, such as the baud rate, data bits, parity bits, and stop bits. To ensure the reliability and security of communication, error detection and validation measures, such as parity checks and CRC checks, need to be implemented. These measures effectively mitigate the occurrence of errors and data inaccuracies that may arise during communication. The soil sensor and STM32 development board employ the Modbus RTU communication protocol. The communication data frame formats are outlined in Tables 1 and 2.

Table 1

Query frame

Address code	Function code	Start Address	Data Length	Check bit low	Check bit high
1byte	1byte	2byte	2byte	1byte	1byte

Table 2

Response frame

Address code	Function code	Valid byte	Data area 1	Data area 2	Data area N	Check code
1byte	1byte	1byte	2byte	2byte	2byte	2byte

When utilizing this protocol for data transmission, it is imperative to initialize the system and configure the 485 interfaces for transmission mode. Subsequently, the host sends a query frame to the slave sensor. Upon receiving the query frame, the slave responds with an acknowledgment frame. At this point, the host's receive buffer is cleared, and it switches to receive mode to receive data from the slave.

During the data reception process, the system undergoes a series of checks. Initially, it verifies whether it has received a response from the slave. If a response is received, the system proceeds to confirm whether the received slave address matches 0x01. If the slave address is correct, the system calculates the CRC checksum and compares it with the checksum in the acknowledgment frame. If they match, the system converts the hexadecimal data to decimal and outputs it. In case of a mismatch, the system returns to the initialization phase to resend the query frame.

In this study, programming was performed using the Keil uVision5 software platform, and the entire program flow is depicted in Fig. 3.

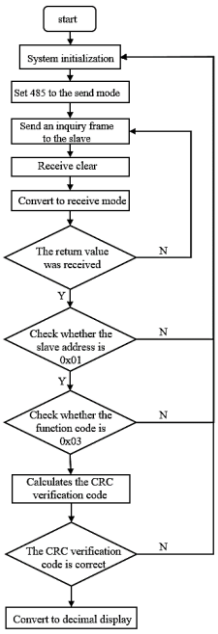

Fig. 3 – Program flow chart

Soil information collection test

To investigate the uniformity of soil nutrient distribution and the impact of sampling density on prescription charts, a rectangular plot measuring 132 meters by 144 meters was selected within the Qianmuyuan Garden Grape Base, located in Huantai County, Zibo City, Shandong Province, China (N37.07420°, E117.91777°).

This site is situated in a temperate monsoon climate region, characterized by yellow-brown soil. The experimental site within the Qianmuyuan Grape Base is of substantial scale and representational significance.

The cultivation pattern in the Qianmuyuan Garden Grape Base follows a ridge-planting approach, where grapevines are planted in a single row on each ridge, with row spacing set at 3 meters.

Bigemap GIS Office software was used to locate the test site through the map query function, as shown in Fig. 4.

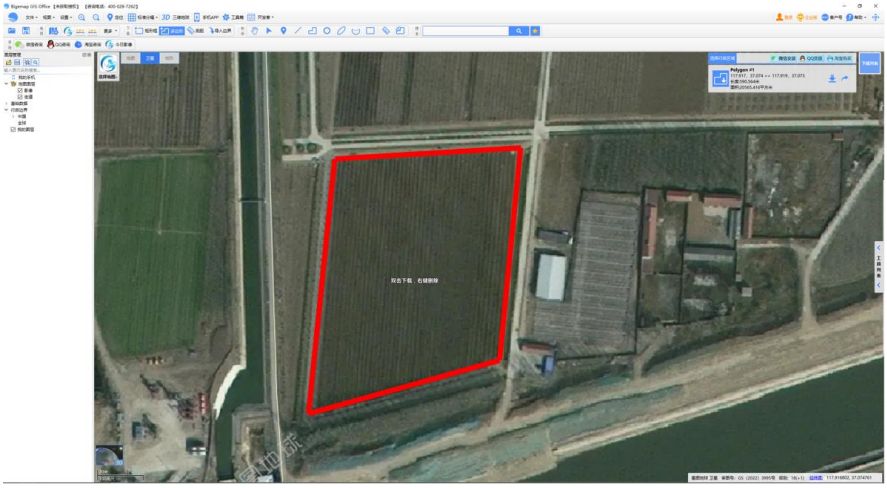

Fig. 4 – The test site

To examine the uniformity of soil nutrient distribution and assess the influence of sampling density on prescription charts, sampling points were selected at various intervals, specifically 1 meter, 3 meters, 6 meters, 9 meters, and 12 meters apart. This equates to a grid pattern of 1m x 1m, 3m x 3m, 6m x 6m, 9m x 9m, and 12m x 12m, respectively, with samples collected at the geometric center of each grid. Each sampling method consisted of 100 samples, resulting in a total of 500 sampling points.

The soil information collection method employed in this study involves selecting sampling points at positions approximately 0.6m away from the grapevine roots, at a depth of 0.2m. Location information is obtained through GNSS-RTK real-time positioning, which offers centimeter-level accuracy. To simultaneously capture both the position information and nutrient content at the sampling points, a sensor is installed on the chassis of a remote-controlled vehicle.

At the front of the vehicle, a drilling device is mounted, affixed to a rod using 3D-printed fixtures. The up-and-down motion of the electric actuator, controlling the drilling operation, is managed by manipulating the high and low levels of an STM32 microcontroller. The steel needle of the sensor measures 0.07m in length, allowing for the collection of soil information at a depth of 0.2m. By controlling the electric actuator, the drilling device creates a hole with a depth of 0.13 meters to reach the required depth. Additionally, GNSS-RTK is used to connect the computer and serial port assistant software, enabling real-time acquisition of the sampling point's location information.

Fig. 5 – Soil collection test

The Christiansen uniformity coefficient is an indicator used to measure the uniformity of nutrient distribution in soil. It effectively reflects the deviation of nutrient distribution across the field from the mean value. This coefficient is calculated by assessing the differences between nutrient content at each sampling point and the mean value, followed by a standardization process. A higher numerical value indicates a more uniform distribution of soil nutrients, whereas a lower value suggests non-uniformity. The formula for calculating the Christiansen uniformity coefficient is as follows:

$$C_{uc} = 100 * \left(1 - \frac{\sum_{i=1}^{n} \left| w_i - \overline{w} \right|}{\sum_{i=1}^{n} w_i} \right) \quad (1)$$

where:

C_{uc} is Christiansen uniformity coefficient; n is the number of soil sampling sites; w_i is nutrient content at the i soil sampling site; $\overline{w}$ is the average nutrient content of the soil sampling site.

The soil nutrient data at various sampling densities were extracted, and the Christiansen Uniformity Coefficient for different sampling densities was computed using Equation (4), yielding the results as presented in Table 4.

Table 4

Christiansen uniformity coefficient at different sampling densities

Sampling density	Christiansen uniformity coefficient		
(m×m)	Rapidly available nitrogen	Rapidly available phosphorus	Rapidly available potassium
12×12	76.11%	77.58%	78.07%
9×9	82.89%	81.71%	83.18%
6×6	86.80%	85.96%	87.77%
3×3	88.32%	87.13%	88.59%
1×1	90.03%	89.03%	90.38%

From the data presented in Table 4, it is evident that, as the sampling density decreases below 6m x 6m, the soil's readily available nitrogen content remains stable within the range of 85% to 91% when compared to denser sampling densities. Similarly, the readily available phosphorus content stabilizes within the range of 85% to 90%, while the readily available potassium content stabilizes within the range of 87% to 92%. These findings indicate a relatively close uniformity in nutrient distribution among different sampling densities.

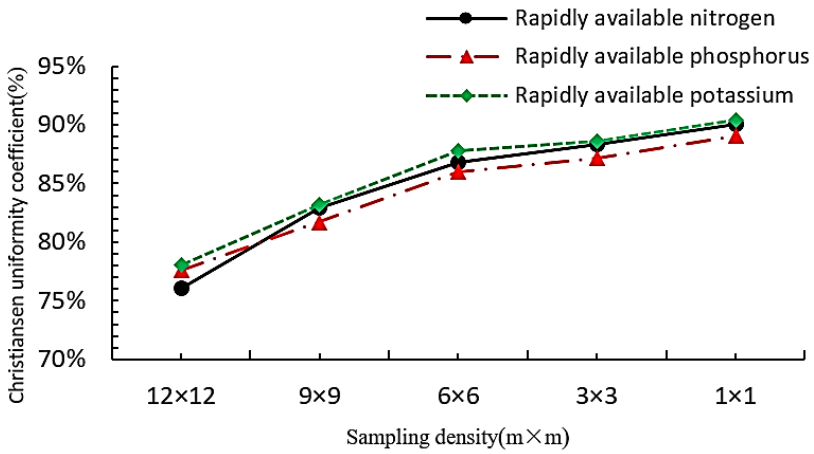

Fig. 6 – Variation map of nutrient distribution uniformity

Moreover, as illustrated in Fig 6, it can be observed that starting from the 12m x 12m sampling density, with an increase in sampling density, the uniformity of nutrient distribution gradually improves. At a sampling density of 6m x 6m, all three nutrient profiles exhibit a turning point, beyond which the slope of the curves noticeably decreases, indicating a reduction in the rate of uniformity change. Therefore, a sampling density of 6m x 6m can be employed for experimentation.

Subsequently, with a sampling density of 6m x 6m, a total of 378 sampling points were re-sampled, and the distribution of these sampling points is depicted in the following Fig. 7.

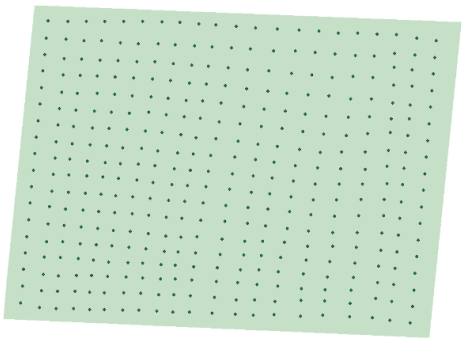

Fig. 7 – Distribution of sampling points

The experimental data obtained with a grid sampling density of 6m x 6m are presented in Table 5. From the data in Table 5, it can be observed that the coefficient of variation for readily available nitrogen, phosphorus, and potassium distribution in the experimental area is approximately 20%, indicating a relatively low level of variation and relatively uniform distribution. The kurtosis values are 5.4425, 5.4027, and 5.1216, all of which exceed the kurtosis of 3 for a normal distribution. This suggests that, compared to a normal distribution, the probability density distribution curves for these three elements have sharper peaks and are steeper. The skewness for all three elements is greater than zero, indicating a leftward skewness in data distribution compared to a normal distribution. This implies the presence of significant outliers, with a long tail trailing on the right side in the histogram, which corresponds to areas in the experimental field with higher levels of readily available nitrogen, phosphorus, and potassium content.

Table 5

Christiansen uniformity coefficient at sampling density 6m × 6m

Item	Minimum value [mg/kg]	Maximum value [mg/kg]	Md-value [mg/kg]	Mean value [mg/kg]	Standard deviation [mg/kg]	Coefficient of variation [%]	Kurtosis	Skewness
N	6	31	17	16.643	3.4782	20.8989	5.4425	0.73429
P	13	41	23	23.751	5.4953	23.1371	5.4027	1.2861
K	29	101	54.5	56.841	13.883	24.4243	5.1216	1.2943

A grid sampling density of 6m x 6m strikes a favorable balance between data precision and the labor costs associated with sampling. In comparison to higher-density sampling, it reduces the workload involved in data collection and processing, while simultaneously offering improved data precision relative to lower-density sampling.

Establishment of soil nutrient distribution map

Since the collected soil nutrient data and coordinate points are discrete, obtaining continuous demand values for readily available nitrogen, phosphorus, and potassium within the field requires the conversion of point data into spatial data through interpolation methods.

The Ordinary Kriging method, suitable for flatland areas, is employed to transform the discrete point-based data into spatial data *(Li et al., 2012)*. The calculation formula for this method is as follows:

$$\hat{Z}(S_0) = \sum_{i=1}^{N} \lambda_i Z(S_i) \quad (2)$$

where:

$\hat{Z}(S_0)$ is estimated value of point(x_0,y_0); λ_i is the unknown weight of the measured value at position i; S_0 is predicted position; N is number of measured values.

The fundamental concept underlying this approach involves treating the neighboring known points of the points to be interpolated as a random field. By seeking the optimal spatial autocorrelation function model to depict the spatial variability of this random field, the model is then used for interpolation at the unknown points.

Based on the soil nutrient content data collected at a sampling density of 6m x 6m and utilizing the Ordinary Kriging interpolation method, the resulting soil nutrient distribution map is presented below, showcasing a gradual increase in nutrient content from 1 to 10.

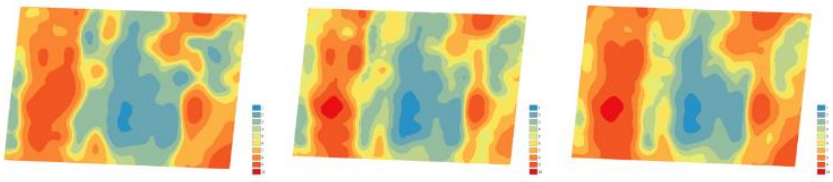

a). Nitrogen *b). Phosphorus* *c). Potassium*

Fig. 8 – The nutrient distribution map

The construction and experimental methods of the fertilization system

In order to test whether the adjustable fertilizer application range of the device and the control system can meet the requirements of fertilizer application, and to verify the accuracy and stability of variable fertilization, laboratory experiments were carried out.

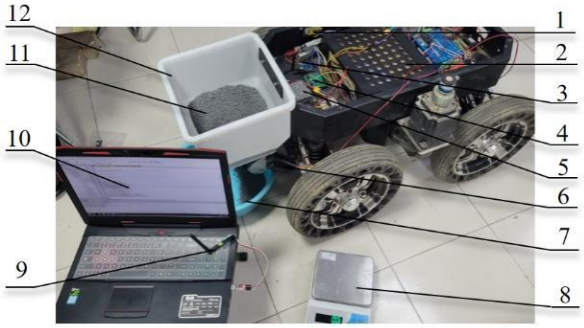

Fig. 9 – Variable fertilization laboratory test

1. Stm32 development board; 2. 48V vehicle power supply; 3. Wireless transmission module; 4.stm32 development board; 5. 48V to 12V step-down module; 6. Fertilizer motor; 7. Plastic basin; 8. Electronic scale; 9. Wireless transmission module; 10. Computer; 11. Fertilizer; 12. Fertilizer box

The indoor simulated variable fertilization experiment is shown in Fig 9. The discharge amounts of urea, superphosphate and potassium nitrate were calibrated at 8, 16, 24, 32, 40, 48, 56, 64 and 72 r/min with the fertilizer dispenser. The relationship between fertilizer discharge and rotational speed of three kinds of fertilizers was studied.

RESULTS

Application of soil fertilization prescription map in variable fertilization

The primary methods for determining fertilization quantities include the Nutrient Balance Method, the Nutrient Surplus/Deficiency Index Method, and the Fertilizer Response Function Method, each of which has its own advantages and disadvantages. The Nutrient Balance Method estimates soil fertilizer supply by measuring soil nutrient content and basic yield. Among these three methods, this approach is better suited for this experiment, where fertilizer quantities are determined through soil nutrient testing. The formula for calculation is as follows:

$$U_N = \frac{V_N S - 0.16\omega_s \mu_N}{\omega_f \eta_{Nf}} \quad (3)$$

where: U_N is rate of fertilizer application; V_N is nutrient uptake per unit yield of crop; S is target yield. (The 3-year average yield of local crops is increased by 10% to 15%); 0.16 is the conversion coefficient represents the nutrient coefficient that the soil available nutrients can be converted into the arable layer of each mu of land; ω_S is soil available nutrient test value; μ_N is correction coefficient of available nutrient; ω_f is nutrient content in fertilizer; η_M is fertilizer utilization rate.

Through consultation with local experts in grape cultivation, it has been determined that for every 100kg of grape fruit production, the absorption of pure nutrients is as follows: 0.6 kg of nitrogen (N), 0.3 kg of phosphorus (P_2O_5), and 0.72 kg of potassium (K_2O). Urea contains 46% nitrogen (N), calcium superphosphate contains 16% phosphorus (P_2O_5), and potassium chloride contains 60% potassium (K_2O).

The soil available nutrient correction factors are set as follows: in the unfertilized area, the nutrient quantity absorbed by crops per hectare is multiplied by 100%.

Generally, the soil available nutrient correction factors fall within the range of 0.3 to 0.7 for available nitrogen, 0.4 to 0.5 for available phosphorus, and 0.5 to 0.85 for available potassium. The arithmetic mean between the maximum and minimum values is taken. Nutrient utilization efficiency is typically in the range of 20% to 40% for nitrogen, 15% to 25% for phosphorus, and 40% to 60% for potassium. Again, the arithmetic mean between the maximum and minimum values is used, resulting in nitrogen fertilizer utilization of 30%, phosphorus fertilizer utilization of 20%, and potassium fertilizer utilization of 50%.

The calculated fertilizer quantities are divided into five equal levels, corresponding to five different application rates. Three types of fertilizers (urea, calcium superphosphate, and potassium chloride) are applied using a fertilizer distributor at different rotational speeds to calibrate the application rates.

The spacing between ridges in the experimental area is approximately 3 meters, and the distance between grape trees is approximately 1.5 meters. Consequently, a grid of 1.5m x 3m is superimposed on the nutrient distribution map, where each grid represents a fertilization unit. Using the lower-left corner of the study area as the origin, a Y-axis is drawn to the upper-left corner to determine the grid's row width and row height, thereby creating the grid. Subsequently, the obtained grid and the points within each grid are clipped to fit within the study area, as depicted in Fig 10.

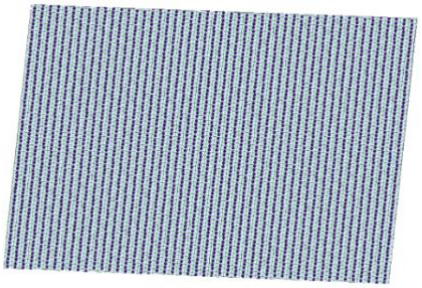

Fig. 10 – Clipped grid

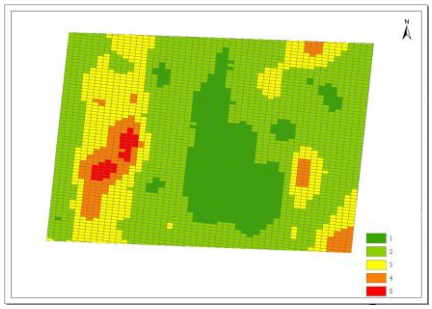

Fig. 11 – Fertilization prescription chart of nitrogen

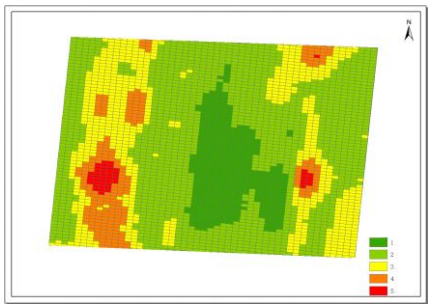

Fig. 12 – Fertilization prescription chart of phosphate

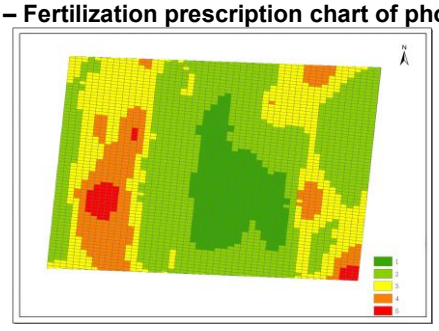

Fig. 13 – Fertilization prescription chart of potassium

As shown in Fig. 11 to Fig. 13, fertilization level 1 corresponds to the regions within the nutrient distribution map with lower nutrient content, resulting in the maximum required fertilizer application, and so forth, with fertilization level 5 requiring the least amount of fertilizer.

Soil nutrient levels directly affect crop yield *(Li et al., 2022)*, so the variation of nutrients in different regions is the starting point and basis for variable fertilization. The exported prescription chart in CSV format is wirelessly transmitted from the computer to the onboard microcontroller via a wireless communication module. Upon receiving the prescription chart information, the microcontroller calculates the desired fertilizer quantities for urea, calcium superphosphate, and potassium chloride at its current location. Subsequently, this information is transmitted to the fertilizer distribution shaft control motor, allowing for the adjustment of the distribution shaft's rotational speed. This process enables variable-rate fertilization operations, as illustrated in Fig. 14.

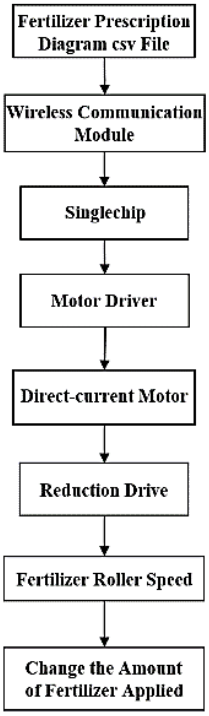

Fig. 14 – Flow chart of variable fertilizer control system

Laboratory test of fertilization system

During calibration, a plastic basin is placed under the fertilizer box, and the fertilizer is weighed by an electronic scale. Each fertilizer was tested for 10 times at each speed. The unitary linear regression analysis was carried out on fertilizer discharge and rotational speed, and the unitary linear regression model between fertilizer discharge and rotational speed was obtained:

$$M_f = an + b \tag{4}$$

where: M is the fertilizer discharge per minute of the fertilizer dispenser, n is the rotation speed of the fertilizer wheel, and a,b is the coefficient and constant of the unitary linear regression model. The a,b values corresponding to the three fertilizers are different.

Table 6

Regression results and significance test

	a	b	R^2	P-value
urea	29.644	357.95	0.9827	2.84×10-6
superphosphate	65.328	382.65	0.9915	6.71×10-7
potassium	34.004	-26.375	0.9893	1.04×10-6

As can be seen from Table 6, the determination coefficient R^2 of the linear regression model established by the fertilizer discharge amount of three fertilizers and the rotation speed of the fertilizer discharge wheel is no less than 0.98, and the P value is less than 0.0001. Therefore, the linear regression equations established between the fertilizer discharge amount of three fertilizers and the rotation speed of the fertilizer discharge wheel are particularly significant and have a high degree of fit, showing a linear relationship with a confidence of 99.99%.

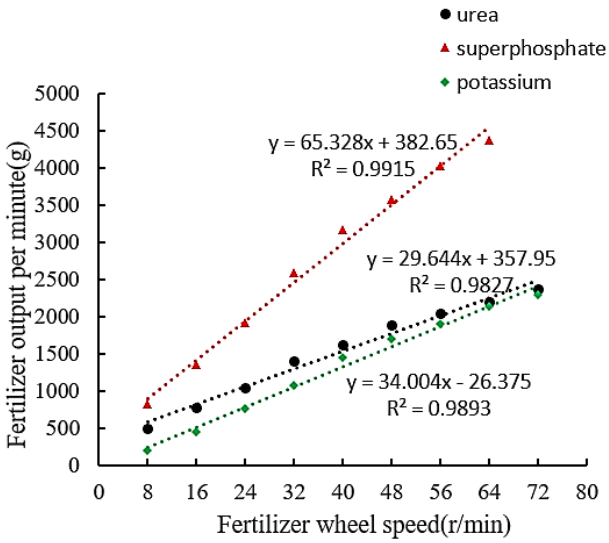

Fig. 15 – Relationship between fertilizer discharge and speed change

The amount of fertilizer applied by each fertilizer is calculated through the prescription diagram, and the corresponding rotation speed of the fertilizer wheel can be obtained by bringing it into the regression equation. Then variable fertilization can be carried out by adjusting the PWM duty ratio to reach the required rotation speed.

In summary, the use of prescription diagrams to calculate fertilizer application rates, coupled with adjusting the rotation speed of the fertilizer wheel through regression equations, has enabled variable-rate fertilization. This method, achieved through PWM duty ratio adjustments, provides a precise means of achieving the required rotation speeds. These findings are crucial for advancing precision agriculture practices. However, further research is needed to compare these results with those from other countries or regions to gain a comprehensive understanding of variable-rate fertilization systems worldwide.

CONCLUSIONS

This study proposed an effective variable fertilization method by integrating soil sensor technology and geographic information systems, providing technical support and theoretical guidance for agricultural production.

An indoor fertilization experiment was conducted, and a linear regression equation was established between the discharge of three types of fertilizers and the rotation speed of the fertilizer wheel to further guide variable fertilization. The results of this study are of great significance for improving the efficiency of fertilization in vineyards, reducing fertilization costs, and promoting the development of precision agriculture.

ACKNOWLEDGMENT

This work was supported by the Natural Science Foundation of Shandong Province, No. ZR202111290044 and Shandong Province Modern Agricultural Industrial Technology System Innovation Team Project (SDAIT-02-02).

REFERENCES

[1] An X., Fu W., Wei X., et al. (2017). Evaluation of Four-element Variable Rate Application of Fertilization Based on Maps (基于处方图的垄作玉米四要素变量施肥机作业效果评价). *Transactions of the Chinese Society for Agricultural Machinery*, Vol. 48, Issue S1: 66-70.

[2] Bai Q., Zhang X, Luo H., et al. (2021). Control system for auto-targeting precision variable-rate fertilization of fruit trees in a greenhouse orchard (设施果园自动对靶精准变量施肥控制系统). *Transactions of CSAE*, Vol. 37, Issue 12: 28-35.

[3] Chung S.O., Kabir M.S.N, Kim Y.J. (2018). Variable Fertilizer Recommendation by Image-based Grass Growth Status. *IFAC-PapersOnLine,* Vol. 51, Issue 17: 10-13.

[4] Jin X., Li Q., Yuan Y., et al. (2018). Design and Test of 2BFJ-24 Type Variable Fertilizer and Wheat Precision Seed Sowing Machine (2BFJ-24 型小麦精量播种变量施肥机设计与试验). *Transactions of the Chinese Society for Agricultural Machinery*, Vol. 49, Issue 05: 84-92.

[5] Kabir M., Chung S., Jang B., et al. (2018). Variable Fertilizer Recommendation by Image-based Grass Growth Status. *IFAC-PapersOnLine*, Vol. 51, Issue 17: 10-13.

[6] Li M., Wen X., Zhou F. (2016). Working Parameters Optimization and Experiment of Precision Hole Fertilization Control Mechanism for Intertilled Crop (中耕作物精准穴施肥控制机构工作参数优化与试验). *Transactions of the Chinese Society for Agricultural Machinery*, Vol. 47, Issue 09: 37-43.

[7] Li X., Liu D., Wang X., et al. (2022). Screening and monitoring of soil fertility stress using ensemble empirical mode decomposition (基于集合经验模态分解算法的土壤肥力胁迫甄别与监测). *Transactions of CSAE*, Vol. 38, Issue 21: 137-146.

[8] Li Z., Zhao G., Zhao Q., et al. (2012). Comparison of Spatial Interpolation Methods for Soil Nutrients in Cultivated Land Fertility Evaluation (县域耕地地力评价中土壤养分空间插值方法的比较研究).*Chinese Agricultural Science Bulletin*, Vol. 28, Issue 20: 230-236.

[9] Liu G., Hu H., Huang J., et al. (2021). Lag Time Detection and Position Correction Method of Variable Rate Fertilization (变量施肥滞后时间检测与位置修正方法研究). *Transactions of the Chinese Society for Agricultural Machinery*, Vol. 52, Issue S1: 74-80.

[10] Marius K., Bručienė I., Jasinskas A., et al. (2021). Comparative analysis of energy and GHG emissions using fixed and variable fertilization rates. *Agronomy*, Vol. 11, Issue 01: 138.

[11] Reyes J. F., Esquivel W., Cifuentes D., et al. (2015). Field testing of an automatic control system for variable rate fertilizer application. *Comput. Electron. Agric.,* Vol. 113, 260-265.

[12] Saleem S., Zaman Q., Schumann A., et al. (2013). Impact of variable rate fertilization on subsurface water contamination in wild blueberry cropping system. *Applied engineering in agriculture*, Vol. 29, Issue 2: 225-232, United States.

[13] Shi Y., Chen M., Wan X., et al. (2017). Analysis and Experiment of Fertilizing Performance for Precision Fertilizer Applicator in Rice and Wheat Fields (稻麦精准变量施肥机排肥性能分析与试验). *Transactions of the Chinese Society for Agricultural Machinery*, Vol. 48, Issue 07: 97-103.

[14] Xu X., Zhang H., Xi L., et al. (2011). Decision-making System for Wheat Precision Fertilization Based on WebGIS (基于 WebGIS 的小麦精准施肥决策系统) *Transactions of CSAE*, Vol. 27, Issue S2: 94-98.

[15] Yang S., Yang W., Wang Y. (2010). Remote Collecting and Monitoring System of Soil Moisture Content Information. *Transactions of the Chinese Society for Agricultural Machinery*, Vol. 41, Issue 9: 173-177.

[16] Yang C. (2001). A variable rate applicator for controlling rates of two liquid fertilizers *Applied engineering in agriculture*, Vol. 17, Issue 3: 409.

[17] Yuan J., Liu Q., Liu X., et al. (2014). Granular Multi-flows Fertilization Process Simulation and Tube Structure Optimization in Nutrient Proportion of Variable Rate Fertilization (多肥料变比变量施肥过程模拟与排落肥结构优化). *Transactions of the Chinese Society for Agricultural Machinery*, Vol. 45, Issue 11: 81-87.

[18] Yuan Y., LI S., Fang X., et al. (2013). Decision Support System of N, P and K Ratio Fertilization (氮磷钾配比施肥决策支持系统) *Transactions of the Chinese Society for Agricultural Machinery*, Vol. 44, Issue 08: 240-244+223.

[19] Zhai C., Yang S., Wang X., et al. (2022). Status and Prospect of Intelligent Measurement and Control Technology for Agricultural Equipment (农机装备智能测控技术研究现状与展望). *Transactions of the Chinese Society for Agricultural Machinery*, Vol. 53, Issue 04: 1-20.

[20] Zhang J., Yan S., Ji W., et al. (2021). Precision Fertilization Control System Research for Solid Fertilizers Based on Incremental PID Control Algorithm (基于增量式 PID 算法的多种固体肥精确施控系统研究). *Transactions of the Chinese Society for Agricultural Machinery*, Vol. 52, Issue 03: 99-106.